Available online at www.sciencedirect.com
ScienceDirect
Catalysis Today 126 (2007) 37–43
CATALYSIS TODAY
www.elsevier.com/locate/cattod

Application of multinuclear MRI and solid state MRI in heterogeneous catalysis

Igor V. Koptyug [a,*], Anna A. Lysova [a], Renad Z. Sagdeev [a], Valentin N. Parmon [b]

[a] International Tomography Center, Institutskaya St. 3A, Novosibirsk 630090, Russia
[b] Boreskov Institute of Catalysis, Pr. Akademika Lavrentieva 5, Novosibirsk 630090, Russia

Available online 21 November 2006

Abstract

This paper presents some of the existing applications of the NMR imaging (MRI) technique relevant to catalytic research. Through the examples presented, it is demonstrated that MRI is a powerful addition to other modern techniques employed to characterize properties of catalysts and catalytic reactors and their performance. It is shown that the existing MRI approaches can be applied to get insight into a broad range of characteristics of catalysts and reactors. The examples presented include preparation and characterization of porous catalyst supports, dynamic studies of supported catalysts preparation by solution impregnation, packing and structure of catalyst beds and reactors, and various types of mass transport in the catalyst particles as well as in the entire reactor. Last but not least, it is shown that rapid MRI strategies are useful to study dynamic processes in operating catalytic reactors, with the multiphase catalytic hydrogenation reaction at elevated temperatures used as a representative example. These in situ studies demonstrate a number of essential phenomena including ignition of individual catalyst particles and their mutual influence, while combination of the spectroscopic and imaging modalities of the NMR technique can be useful for the characterization of the chemical conversion under reactive conditions.

Keywords: Catalysts preparation; Packed bed reactor; Mass transport; Hydrogenation; In situ MRI

1. Introduction

Nuclear magnetic resonance spectroscopy (NMR) is widely employed in catalytic applications [1,2] and yields information about molecular scale composition, structure and processes, albeit averaged over the entire sample. Its imaging modality, magnetic resonance imaging (MRI) [3], can provide essentially the same information, but with the spatial resolution on the order of tens or hundreds of microns. The advantages of MRI include (but are not limited to) its non-invasive and non-destructive character and chemical specificity. More importantly, MRI allows one to obtain qualitative and quantitative maps of various characteristics such as diffusivity and flow velocity, chemical composition, pore size distribution, temperature and a lot more. This makes MRI a versatile toolkit rather than a single specialized research tool, useful for the characterization of a wide variety of materials and dynamic processes which exhibit heterogeneity on a macroscale as often encountered in chemical engineering and heterogeneous catalysis [4]. It is essential that MRI can be used to perform in situ studies of operating reactors [4,5]. Such applications are not common at present, and many potentially important areas of such applications remain hardly addressed. At the same time, it is already obvious that MRI can be an invaluable technique for catalytic research, and the interest to such applications is rapidly growing. This paper presents some of the existing applications of the MRI technique relevant to catalytic research. In particular, the applicability of MRI to study the preparation and characterization of porous supports and supported catalysts, catalyst bed structure, mass transport processes in the bed and in the individual catalyst particles, and processes taking place in an operating multiphase catalytic reactor is demonstrated.

2. Experimental

Monoliths, cylindrical extrudates and beads made of γ-Al_2O_3 were used in the experiments as model porous media or

* Corresponding author. Tel.: +7 383 3333561; fax: +7 383 3331399.
E-mail address: koptyug@tomo.nsc.ru (I.V. Koptyug).

0920-5861/$ – see front matter © 2006 Elsevier B.V. All rights reserved.
doi:10.1016/j.cattod.2006.10.001

as catalyst supports. In the phosphate transport experiments upon supported catalyst preparation, cylindrical alumina pellets 3.2 mm in diameter and 12 mm long were placed in a 0.76 M aqueous solution of H_3PO_4. For the in situ studies of hydrogenation reaction, catalysts used contained 1% Pd by weight on the γ-Al_2O_3 supports shaped as cylinders 4.5 mm in diameter and 12 mm long, or beads of 1, 2–3, or 4.2 mm in diameter. Before any hydrogenation experiment, individual catalyst pellets were activated in a mixed H_2-air stream with excess of hydrogen. For 1 mm and 2-3 mm beads, the catalyst bed was activated for 30 min in H_2 stream at 450 °C followed by cooling to room temperature in a stream of He. The bed of 4.2 mm beads was activated in a H_2-air stream with excess of hydrogen, then heated to 450 °C in a stream of He, and then cooled back to room temperature without interrupting He stream. After activation, the catalyst was loaded into the home-built MRI-compatible reactor residing inside the NMR magnet. Catalyst beds were often placed on a layer of inert alumina beads of the same size. Liquid α-methylstyrene, *n*-octene-1 and *n*-heptene-1 were used as reactants in the multiphase hydrogenation studies.

All imaging experiments were performed on a Bruker Avance DRX 300 MHz wide bore spectrometer equipped with imaging accessories, at 300.13 MHz (^{1}H), 121.49 MHz (^{31}P), 79.39 MHz (^{23}Na) or 78.2 MHz (^{27}Al). Two-dimensional images were obtained using the 2-pulse spin-echo sequence. All 2D images of individual catalyst pellets and transverse images of catalyst beds were obtained with 230 μm × 140 μm spatial resolution, while for axial images of the bed it was 230 μm × 310 μm. The rapid 2D and 3D imaging of the operating catalyst bed was performed using the multi-echo pulse sequences. Acquisition time of each 2D image was 2.5 s. Each set of five transverse images corresponding to five different layers of a regularly packed reactor was acquired within 30 s, with the five slices imaged sequentially. These five image sets were detected repeatedly for 3.5 h to monitor dynamic processes in the operating reactor. The reactor volume was thermostatted with an external stream of air preheated to 100 °C.

Imaging of solid materials was performed using the α–τ–2α–τ–echo pulse sequence with $\tau \approx 300$ μs and the nominal flip angle $\alpha = 90°/(I + 1/2)$, where I is the nuclear spin of the respective quadrupolar nucleus. The two spatial coordinates were phase encoded by an independent stepwise variation of two pulsed magnetic field gradients. A field of view of $(9.2\ \text{mm})^2$ was imaged with a spatial resolution of $(288\ \mu\text{m})^2$ without slice selection. Further experimental details can be found in the references cited.

3. Results and discussion

Preparation of supported catalysts often begins with the preparation of porous supports (e.g., alumina extrudates). These are usually produced using the wet mass extrusion process. Then the extrudate undergoes drying which, if performed improperly, can ruin the final product. Using MRI, the water content was monitored periodically in alumina monoliths undergoing moist-curing after extrusion [6]. Water loss was found to be most significant during the first 24 h of curing. Variation of the NMR relaxation times of water molecules suggest that free water in larger pores is removed predominantly at this initial stage. An attempt to accelerate the drying process by placing an adsorbent powder into the monolith channels have led to dramatic consequences as demonstrated in Fig. 1. Since only the ^{1}H NMR signal of water is observed in these experiments, dry alumina and dry adsorbent are not expected to contribute to the images detected. Since the adsorbent has become visible in the image shown in Fig. 1, it is a direct indication that some water has redistributed from the pores of the monolith walls to the adsorbent powder within minutes. As can be seen in Fig. 1, this accelerated drying has resulted in a destruction of the monolith. It was caused by the large gradients of capillary pressure which developed when the fresh extrudate was brought in contact with the adsorbent powder. Therefore, slow water removal is essential for preserving the integrity and shape of the support at the early stages when water content in the extrudate is high. At the subsequent stages, monoliths were dried and then calcined at elevated temperatures. Once the solid structure is formed, the pores of alumina monoliths can be saturated with water once again. The spatial resolution of the MRI technique is several microns at best and therefore does not allow one to observe individual pores. Nevertheless, MRI can provide information on pore sizes in the alumina supports produced. In particular, two alumina monoliths calcined at 1200 °C and 600 °C were saturated with water and imaged [6]. The first sample gave a much stronger NMR signal despite the smaller pore volume and thus the lower water concentration in that sample. The reason is that pore sizes influence the NMR signal by altering the NMR relaxation time of water. This means that MRI studies can provide certain useful information on pore sizes in a porous

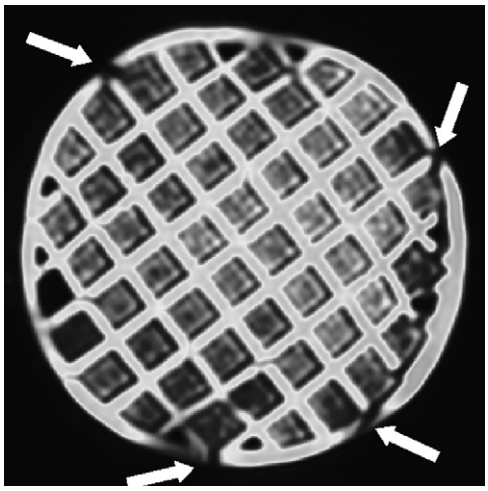

Fig. 1. An extruded alumina monolith with channels filled with alumina powder as an adsorbent. The latter is visible in the image owing to partial water redistribution from the monolith walls to the adsorbent. White arrows show some of the cracks formed due to the action of large capillary pressure gradients during contact drying of the monolith. Lighter shades of gray correspond to higher signal intensity.

sample. The relaxation mediated sensitivity of the observed NMR signal to pore sizes forms the basis of one of the existing approaches to NMR porosimetry [7]. Combination of NMR porosimetry techniques with MRI allows one to obtain local pore size distributions of various porous objects [8].

When the suitable support is available, a supported catalyst can then be prepared by solution impregnation of the support with an active component or its precursor. The transport processes and the interaction of solutes with the porous matrix determine the progress of the impregnation and the final distribution of the active component in the supported catalyst. Therefore, it is important to have means to monitor the preparation process. With conventional techniques, one has to interrupt the process and to cut the support to reveal the distribution achieved at a certain stage of the preparation process. It is obvious that a non-destructive technique capable of following the dynamics of the preparation process on a single support would be useful. We have demonstrated that such non-destructive studies of supported catalysts preparation are feasible with MRI. An earlier example [9] was the preparation of supported Pt/γ-Al_2O_3 (Pd/γ-Al_2O_3) catalysts by impregnating alumina extrudates with an aqueous solution of H_2PtCl_6 (H_2PdCl_4). Pellets with egg-shell and egg-white types of active component distributions were prepared, dried, saturated with cyclohexane and imaged. Comparison of these images with the conventional cut-and-stain approach has demonstrated that cyclohexane relaxation maps qualitatively reproduce the distribution of Pt (Pd) in the extrudates. Relaxation times of water were also found to be sensitive to the presence of $PtCl_6^{2-}$ ($PdCl_4^{2-}$). This allowed us to use MRI to visualize the dynamics of the impregnation process without interrupting it. More recently, we have addressed the preparation of phosphate-promoted (Co)Mo/Al_2O_3 hydrodesulphurization catalysts [10]. Fig. 2 demonstrates that ^{31}P MRI can be used to directly visualize transport of the phosphate in the extrudate. Comparison of the ^{1}H images of water and ^{31}P images of the phosphate have revealed the strong interaction (and therefore slow transport) of the latter with the support. It should be stressed that the images in Fig. 2a and b reflect the spatial distribution of the phosphate in solution only. It is expected that the phosphate adsorbed on the walls of the pores does not contribute significantly to the observed images. The correlation of the spatial distributions of the dissolved and adsorbed phosphate can be established as follows. The impregnation process was interrupted ca. 100 min after its initiation, the pellet was dried, and a ^{31}P image of the phosphate in the solid phase was detected (Fig. 2c). In another experiment, the impregnation process was carried out to the completion, and the pellet was also dried and imaged. As can be seen from Fig. 2d, the liquid and solid phase distributions of the phosphate do indeed correlate, validating the applicability of MRI for the dynamic studies. Transport of paramagnetic cobalt ions cannot be visualized directly with MRI. At the same time, paramagnetic

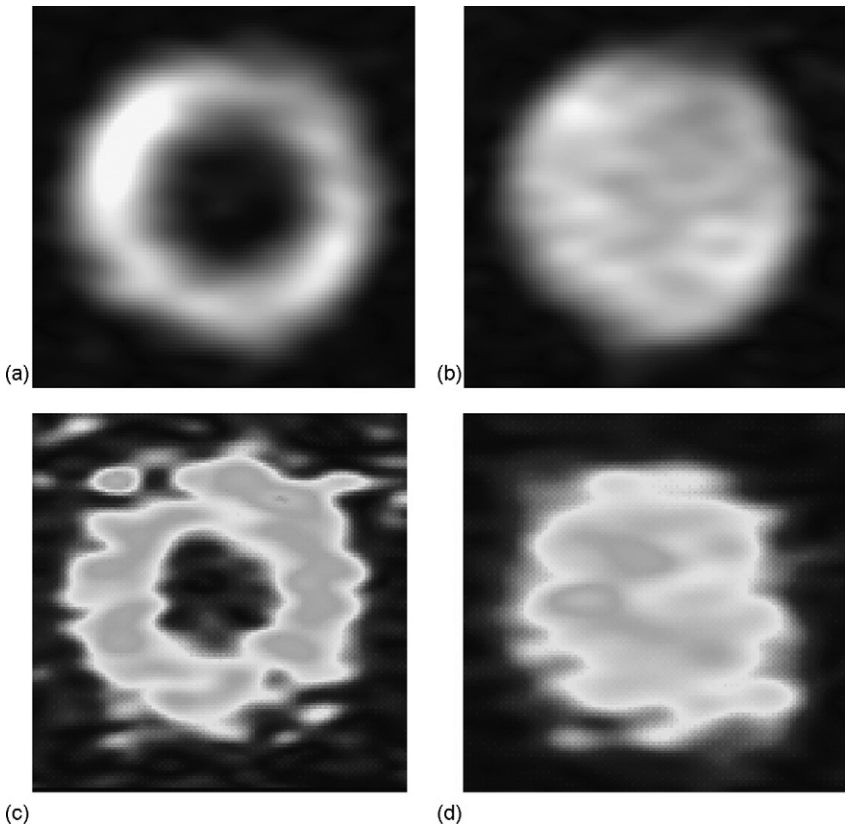

Fig. 2. ^{31}P images demonstrating the distribution of phosphate in alumina pellets. Images a and b visualize distribution of the phosphate in the liquid phase and were detected during the impregnation of the alumina pellet with an aqueous solution of H_3PO_4 ca. 100 min (a) and 18.5 h (b) after starting the process. Images c and d reflect the distribution of the phosphate in the solid phase and were detected after terminating the impregnation ca. 100 min (c) and 18.5 h (d) after starting the impregnation process and drying the pellets. Lighter shades of gray correspond to higher signal intensity.

solutes substantially reduce NMR relaxation times of the solvent (water). Therefore, their transport can be visualized by detecting ^{1}H images of the pellet during impregnation. This has been demonstrated in the impregnation of an alumina pellet with an aqueous solution of $Co(NO_3)_2$ [11]. The images detected have revealed the dynamics of cobalt permeation into the pellet and the influence of the solution pH and the addition of citric acid on the rate of permeation and the achieved distribution of Co^{2+} within the pellet. Transport of molybdenum was studied during impregnation of an alumina pellet with an aqueous solution of $(NH_4)_6Mo_7O_{24}$. Similar to the results obtained earlier for Pt/Al_2O_3, impregnation with molybdate leads to the increase of the NMR relaxation times of water. This can be used for a selective visualization of either the Mo-containing or the Mo-free regions of the pellet under study [11]. At the same time, detecting images using the NMR signal of ^{95}Mo can be potentially used for a more direct visualization of molybdenum transport. Direct imaging of Pt distribution was demonstrated during the impregnation of alumina pellets with an aqueous solution of H_2PtCl_6 by detecting the ^{195}Pt NMR signal [10].

Once the supported catalyst is available, it has to be packed, e.g., in a packed bed reactor. The details of the fixed bed structure are of paramount importance since even small variations in the bed structure have been shown to produce a significant impact on the reactor performance. The conventional approach to the visualization of the structure of a packed bed by MRI is indirect. It is based on the detection of the NMR signal of a liquid saturating the catalyst pellets or filling the inter-pellet voids, as demonstrated in Fig. 3. However, quite recently we have shown that a more direct approach is feasible, based on the direct multinuclear solids imaging. In particular, alumina extrudates and alumina and cordierite monoliths were imaged successfully using ^{27}Al NMR signal detection and conventional (liquids) NMR hardware and techniques [12,13]. As an example, Fig. 4 demonstrates an image of a fragment of alumina monolith with 2 mm × 2 mm channels and ca. 0.5 mm

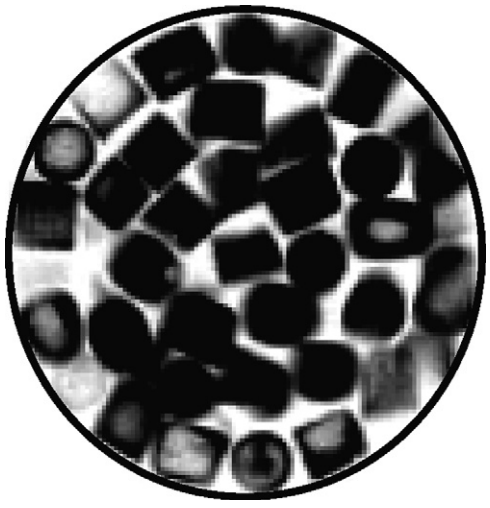

Fig. 3. 2D image of a bed of cylindrical alumina extrudates partially saturated with water and packed in a glass cylinder. The orientation of individual pellets and their mutual positions are clearly seen in the image. Darker shades correspond to higher signal intensity.

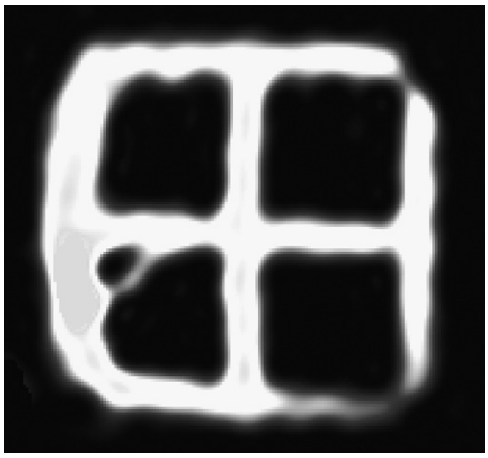

Fig. 4. 2D image of a fragment of a γ-alumina monolith detected using the ^{27}Al NMR signal of alumina. The image was detected in 17 min.

thick walls. The wall on the left appears slightly curved and is thicker than the other walls. This is a true feature of the imaged fragment which was cut out of a bigger cylindrical monolith, with the curved wall corresponding to the outer wall of the original monolith. The use of other magnetic nuclei allowed us to image other ceramic materials and glass. In Fig. 5, 2D ^{23}Na images of a model single-file ''packed bed'' of glass beads and its 3D structure reconstruction are shown. The 2D images show both the beads and the encapsulating glass tube, while the latter is removed from the 3D image for clarity. These results demonstrate that direct multinuclear imaging of the solid phase can potentially become an important tool in the MRI toolkit for chemical engineering and catalytic studies.

Mass transport processes often govern the overall performance of a catalytic reactor. The MRI toolkit has several tools to study transport, and in fact this is the most developed area of MRI applications [3]. Flow maps depicting flow velocities with spatial resolution were obtained for a wide range of flow geometries, from simple circular channels to monoliths and packed beds. Some of us have demonstrated that flow imaging of gases (e.g., propane, butane, acetylene) is also feasible, at least for a laminar flow regime [14–16]. Several interesting developments followed, including flow MRI of turbulent gas flow [17], measurements of spatially resolved gas adsorption isotherms [18] and porous media permeability [19]. It was also shown that gas transport in packed beds can be monitored by detecting the so-called average propagators, employing the PFG NMR technique [15,16] conventionally used to measure diffusivities of various fluids. The propagators are essentially the travel distance probability density functions. They can be measured both along and perpendicular to the average flow direction in a packed bed and for various travel times, from a few ms to a few seconds. This approach was used to evaluate average flow velocity and dispersion coefficients (both axial and transverse) and their long-time asymptotic values for gas filtration in model packed beds [16]. The same approach was proven useful [20] when studying the filtration of solids fines through a packed bed—a process that is sometimes used to intensify heat exchange in a packed bed or for selective

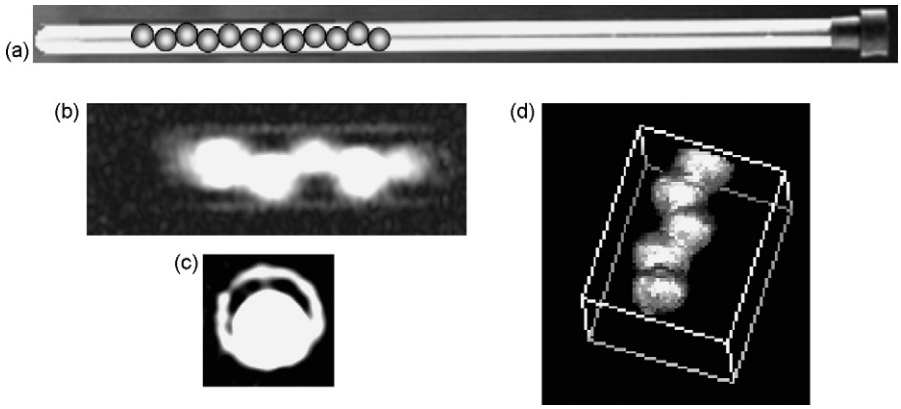

Fig. 5. (a) Schematic representation of the model sample comprising 3.0 mm glass beads in a 5 mm (4.2. mm i.d.) glass NMR tube. The axial (b) and transverse (c) 2D images were detected using the ^{23}Na NMR signal of glass and show both the beads and the tube walls. (d) Reconstruction of the 3D structure of the model sample from the MRI data, with the tube walls intentionally removed to reveal the bead packing.

adsorption and removal of the target product from the reactor to increase conversion. MRI is a useful technique to visualize transport in the porous pellets as well. As model processes, both drying of water-saturated pellets and packed beds [21–23] as well as sorption of water by individual sorbent pellets, packed beds and consolidated layers [24–26] were considered. In all cases, MRI was able to map the spatial distribution of the fluid in the porous matrix and to follow the dynamics of the processes under study. Mathematical modeling of the experimental results was used to evaluate quantitative characteristics of mass transport, such as effective fluid diffusivity in the porous matrix which was generally found to be concentration-dependent. Drying of a water-saturated monolith was used to assess the external mass transport across the interface between the porous walls and the gas streams flowing along the monolith channels [22,25]. It was found that the drying rate rapidly drops as the distance from the inflow edge of the monolith increases, reflecting the convergence of the flow pattern to the fully developed flow along the channels.

The results presented above were obtained in the absence of any catalytic reaction. While such studies are important for an understanding of the catalyst and reactor properties and of the processes taking place within them, the interest of researchers is gradually shifting to the in situ and Operando studies of catalytic processes. The reason is that many properties and processes change dramatically once the reaction is started. While the conventional MRI is unlikely to ever have the ability to address a single active catalytic center, it nevertheless can be employed in the Operando studies and can provide useful information on the state of a catalyst and reactor and on the processes taking place in them. Furthermore, such studies can be performed on the length scales from sub-pellet size to the entire reactor or a substantial part thereof. In particular, MRI is best suited for the studies of the distribution of the liquid phase in gas–liquid–solid catalytic reactors. For our studies, we have considered hydrogenation of unsaturated hydrocarbons (α-methylstyrene (AMS), *n*-heptene-1, *n*-octene-1) on a Pt/Al_2O_3 or Pd/Al_2O_3 catalysts at elevated temperatures. The reaction was chosen both for its importance in industry and a wide use as a model catalytic process. For these studies, an NMR-compatible reactor has been built which enables us to perform catalytic hydrogenation at temperatures up to 100 °C without damaging the spectrometer hardware [4,27–29]. Despite the limited size of the reactor volume (the sensitive zone is ca. 1 cm in diameter and ca. 3–4 cm long), temperature rises of the catalyst up to 250 °C were observed in some experiments. In a very first study of this kind [28], we have mapped distribution of the liquid phase in a single catalyst pellet under reactive conditions for various regimes of this single-pellet reactor operation. At that time, the detection of each 2D image took over 4 min, precluding dynamic studies. Since then, however, we were able to bring the imaging time down first to 0.5 min and then to 2–3 s per 2D image. This resulted in the visualization of a number of dynamic processes in the operating reactor. In a single pellet reactor, the existence of oscillating regimes under unchanged external conditions has been demonstrated [29,30]. The radial or axial reciprocating motion of the liquid front inside the catalyst pellet partially filled with the reactant has been visualized in the course of AMS hydrogenation reaction. These pulsations were accompanied by pellet temperature oscillations, revealing a complex interaction of mass and heat transport processes with the chemical transformation. Radial pulsations are observed for large liquid contents of the pellet and resemble particle ignition due to autocatalytic acceleration of the exothermic hydrogenation process. It was possible to model the oscillating behavior using a set of coupled differential equations which take due account of heat and mass transfer, phase transitions and chemical transformation [31].

Similar studies were performed for the fixed catalyst beds with a varying particle-to-reactor diameter ratio and superficial liquid velocities [32]. In all cases, dynamic images of the liquid phase distribution under operating conditions were detected. In particular, a number of studies have been performed on a regularly packed granular catalyst bed comprising uniform catalyst beads a few mm in diameter. Liquid reactant was supplied to the top of the bed through a thin capillary. All experiments have demonstrated that despite the regular character of the catalyst beads packing, the distribution of the liquid phase in the bed is highly non-uniform, and that the steady state distribution of liquid within the bed changes if the supply of the liquid reactant to the top of the bed is interrupted

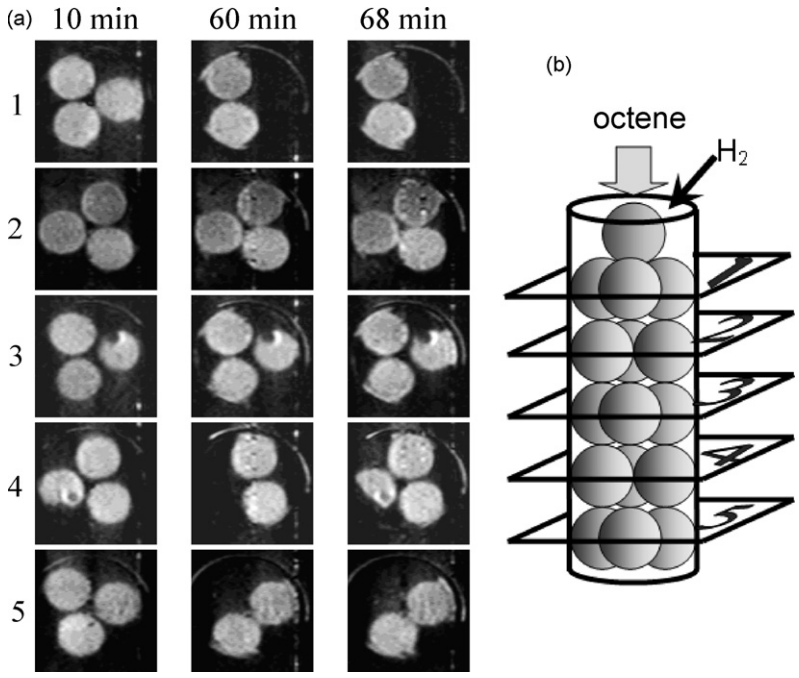

Fig. 6. (a) 2D ^{1}H images of the liquid phase distribution in a regularly packed bed of spherical catalyst beads (Pd/Al_2O_3, 4.2 mm in diameter) detected in the course of octene-1 hydrogenation. Rows 1–5 correspond to the respective layers of the catalyst beads shown schematically in (b). Each column of the images represents a subset of the entire set of images detected for an extended period of time for visualizing dynamic processes in the reactor. The time elapsed from the reactor startup is indicated above the columns of images. Lighter shades correspond to higher signal intensity.

and then resumed. For beads 4–5 mm in diameter, images have revealed the existence of partially filled or completely dry pellets in the operating reactor as well as the ignition of the individual catalyst beads and of the entire catalyst bed. As an example, Fig. 6 shows the results obtained for a regularly packed bed of 15 catalyst beads arranged in five horizontal layers with three beads in each layer. One alumina bead containing no metal catalyst was placed at the top to serve as a distributor of reactant supply. The images in Fig. 6a demonstrate the ignition of individual catalyst beads in the top and in the two bottom layers during the experiment. These beads disappear from the image completely or partially since only the liquid-filled catalyst particles and their parts are observed in the images. In layer 4, the rightmost image demonstrates that one of the beads is partially filled with the liquid phase which it imbibes from its neighbors. Such states were observed to persist for long periods of time, with some oscillating motion of the liquid front similar to that described above for single-pellet reactors. The existence and thus observation of such states is only possible in the Operando mode and reflects mutual coupling of mass transport, heat transport and phase transitions with the chemical reaction. In the absence of the chemical reaction, capillary forces rapidly redistribute the liquid phase within the catalyst beads toward a uniform spatial distribution of the liquid phase. Such partially filled beads should be most efficient in performing the reaction since they have a substantial supply of the liquid reactant which evaporates readily and undergoes a facile gas phase hydrogenation on the dry exposed surface of the catalyst. The results obtained imply that phase equilibrium during an exothermic reaction can be violated locally making the reactor prone to runaway.

Since NMR is a powerful spectroscopic technique, combining NMR and MRI approaches it is possible to obtain spatially resolved NMR spectra and thus to evaluate the local degree of chemical conversion. Despite the significant broadening of the NMR spectra of liquids permeating porous solids, NMR spectra obtained for each volume element of an image can still provide quantitative information about the local chemical conversion in an operating reactor, especially if the reaction is carried out at elevated temperatures. In particular, in the studies of AMS hydrogenation, the relative amounts of AMS and reaction product cumene have been mapped during the reaction inside the trickle bed reactor. These experiments have revealed both axial and radial conversion variations within the catalyst bed [4,29].

4. Conclusions

The MRI toolkit is a powerful addition to other modern techniques which are used to characterize properties of catalysts and catalytic reactors and their performance. MRI has its disadvantages as well as advantages, but the development of many new applications of MRI in catalytic research is just being initiated. Nevertheless, several examples presented above are intended to demonstrate that the applications which have already been attempted clearly show the potential of MRI to provide important information on many aspects of catalysts production, utilization, deactivation and regeneration. In particular, there is a growing trend in performing in situ MRI studies of various

operating chemical and biochemical reactors. In particular, visualization of the liquid phase distribution in a trickle bed reactor at different lengthscales, from individual catalyst particles to the entire bed, provides information on the degree of wetting of the catalyst, mechanisms of liquid transport within the reactor, mutual influence of the neighboring catalyst particles, local phase equilibria, and local chemical conversion. Rapid imaging techniques provide access to the visualization of dynamic processes such as catalyst particle ignition and oscillating behavior observed experimentally. Such in situ studies of the coupled heat and mass transfer, phase transitions and chemical conversion are essential for a detailed understanding of the reactor operation and the mechanisms of the development of critical operation regimes. Novel developments in the field of non-medical applications of the MRI technique, such as the direct multinuclear imaging of solid materials, will enable the researchers to add novel tools for in situ and Operando studies of the operating catalytic reactors.

Acknowledgements

This work was partially supported by RFBR (#05-03-32472), RFBR-NWO (03-03-89014-NWO, 047.015.006), RAS (#5.2.3 and 5.1.1), SB RAS (integration grant #11), the Russian President's program of support of the leading scientific schools (#NSch-4821.2006.3), and CRDF (RU-C1-2581-NO-04). A.A. Lysova thanks the Russian Science Support Foundation and the Global Energy Foundation for financial support.

References

[1] M. Hunger, W. Wang, Adv. Catal. 50 (2006) 147.
[2] A.T. Bell, A. Pines (Eds.), NMR Techniques in Catalysis, Marcel Dekker, New York, 1994.
[3] P.T. Callaghan, Principles of Nuclear Magnetic Resonance Microscopy, Clarendon, Oxford, 1991.
[4] S. Stapf, S. Han (Eds.), NMR Imaging in Chemical Engineering, Wiley-VCH, Weinheim, 2006.
[5] I.V. Koptyug, R.Z. Sagdeev, Russ. Chem. Rev. 72 (2003) 165.
[6] S.A. Yashnik, Z.R. Ismagilov, I.V. Koptyug, I.P. Andrievskaya, A.V. Matveev, J.A. Moulijn, Catal. Today 105 (2005) 507.
[7] R.M.E. Valckenborg, L. Pel, K. Kopinga, J. Phys. D: Appl. Phys. 35 (2002) 249.
[8] J.H. Strange, J.B.W. Webber, Meas. Sci. Technol. 8 (1997) 555.
[9] L.Yu. Khitrina, I.V. Koptyug, N.A. Pakhomov, R.Z. Sagdeev, V.N. Parmon, J. Phys. Chem. B 104 (2000) 1966.
[10] A.A. Lysova, I.V. Koptyug, R.Z. Sagdeev, V.N. Parmon, J.A. Bergwerff, B.M. Weckhuysen, J. Am. Chem. Soc. 127 (20050) 11916.
[11] A.A. Lysova, I.V. Koptyug, J.A. Bergwerff, B.M. Weckhuysen, in preparation.
[12] I.V. Koptyug, D.R. Sagdeev, E. Gerkema, H. Van As, R.Z. Sagdeev, J. Magn. Reson. 175 (2005) 21.
[13] I.V. Koptyug, A.A. Lysova, Bruker Spin Report, 2006 (accepted).
[14] I.V. Koptyug, S.A. Altobelli, E. Fukushima, A.V. Matveev, R.Z. Sagdeev, J. Magn. Reson. 147 (2000) 36.
[15] I.V. Koptyug, L.Yu. Ilyina, A.V. Matveev, R.Z. Sagdeev, V.N. Parmon, S.A. Altobelli, Catal. Today 69 (2001) 385.
[16] I.V. Koptyug, A.V. Matveev, S.A. Altobelli, Appl. Magn. Reson. 22 (2002) 187.
[17] B. Newling, C.C. Poirier, Y. Zhi, J.A. Rioux, A.J. Coristine, D. Roach, B.J. Balcom, Phys. Rev. Lett. 93 (2004) 154503–154511.
[18] S.D. Beyea, A. Caprihan, C.F.M. Clewett, S.J. Glass, Appl. Magn. Reson. 22 (2002) 175.
[19] M. Bencsik, C. Ramanathan, Magn. Reson. Imaging 19 (2001) 379.
[20] A.V. Matveev, L.V. Barysheva, I.V. Koptyug, V.M. Khanaev, A.S. Noskov, Chem. Eng. Sci. 61 (2006) 2394.
[21] I.V. Koptyug, V.B. Fenelonov, L.Yu. Khitrina, R.Z. Sagdeev, V.N. Parmon, J. Phys. Chem. B 102 (1998) 3090.
[22] I.V. Koptyug, R.Z. Sagdeev, L.Yu. Khitrina, V.N. Parmon, Appl. Magn. Reson. 18 (2000) 13.
[23] I.V. Koptyug, S.I. Kabanikhin, K.T. Iskakov, V.B. Fenelonov, L.Yu. Khitrina, R.Z. Sagdeev, V.N. Parmon, Chem. Eng. Sci. 55 (2000) 1559.
[24] I.V. Koptyug, L.Yu. Khitrina, Yu.I. Aristov, M.M. Tokarev, K.T. Iskakov, V.N. Parmon, R.Z. Sagdeev, J. Phys. Chem. B 104 (2000) 1695.
[25] I.V. Koptyug, L.Yu. Khitrina, V.N. Parmon, R.Z. Sagdeev, Magn. Reson. Imaging 19 (2001) 531.
[26] N.A. Chumakova, N.V. Vernikovskaya, M.M. Tokarev, I.V. Koptyug, L.Yu. Ilyina, Yu.A. Aristov, Chem. Ing. Tech. 73 (2001) 776.
[27] I.V. Koptyug, A.V. Kulikov, A.A. Lysova, V.A. Kirillov, R.Z. Sagdeev, V.N. Parmon, Doklady Phys. Chem. 385 (2002) 158.
[28] I.V. Koptyug, A.V. Kulikov, A.A. Lysova, V.A. Kirillov, V.N. Parmon, R.Z. Sagdeev, J. Am. Chem. Soc. 124 (2002) 9684.
[29] I.V. Koptyug, A.A. Lysova, A.V. Kulikov, V.A. Kirillov, V.N. Parmon, R.Z. Sagdeev, Appl. Catal. A: Gen. 267 (2004) 143.
[30] I.V. Koptyug, A.A. Lysova, A.V. Kulikov, V.A. Kirillov, V.N. Parmon, R.Z. Sagdeev, Magn. Reson. Imaging 23 (2005) 221.
[31] V.A. Kirillov, I.V. Koptyug, A.V. Kulikov, N.A. Kuzin, A.A. Lysova, A.B. Shigarov, V.N. Parmon, Theor. Found. Chem. Eng. 39 (2005) 24.
[32] V.A. Kirillov, I.V. Koptyug, Ind. Eng. Chem. Res. 44 (2005) 9727.